International Journal of Non-Linear Mechanics 43 (2008) 514–520

Contents lists available at ScienceDirect

International Journal of Non-Linear Mechanics

journal homepage: www.elsevier.com/locate/nlm

Analysis of effects of differential gain on dynamic stability of digital force control

L.L. Kovács[a,*], J. Kövecses[b], G. Stépán[c]

[a]HAS-BUTE Research Group on Dynamics of Machines and Vehicles, H-1521 Budapest, Hungary
[b]Department of Mechanical Engineering and Centre for Intelligent Machines, McGill University, 817 Sherbrooke Street West, Montréal, Quebec, Canada H3A 2K6
[c]Department of Applied Mechanics, Budapest University of Technology and Economics, H-1521 Budapest, Hungary

ARTICLE INFO

Article history:
Received 12 April 2007
Received in revised form 4 February 2008
Accepted 8 April 2008

Keywords:
Differential gain
Dynamic stability
Force control
Sampling time

ABSTRACT

The paper presents an analytical investigation of the dynamics of digital force control. A one degree-of-freedom (DoF) mechanical system with low viscous damping is subjected to proportional–derivative (PD) force control. Analytical results are presented in the form of stability charts in the parameter space of sampling time, control gains and mechanical parameters. Simple closed form results include the largest stable proportional gain and the least steady state force error that provide synthesis of mechanical and control system parameter influences for the design of digital force control. Also, a novel analytical explanation is given why even the properly filtered force derivative signal is rarely used in practice, and why the occurring vibrations have frequencies one range smaller than that of the sampling frequency of the digital control.

1. Introduction

Force control in robotic systems has been the subject of intensive investigations in recent years since most robotic operations involve interactions with other objects. Robotic systems are usually equipped with digital controllers, while the dynamic analysis of robotic systems is often treated using continuous-time (analog) approaches and models. The first, and probably the most referenced papers in the field are [1–3]. These papers present the basics of the force control approaches. The stability of a simple digital force control system was analyzed in [1] for the first time.

Simultaneously, comprehensive textbooks [4–7] were published on digital control theory. These works are used as standards in digital realizations of control algorithms, which are usually based on continuous-time arguments. For example, using the frequency response bandwidth or the crossover frequency of the continuous-time system, Refs. [7,8] suggest to determine an appropriate (sufficiently small) sampling period for the discrete-time realization. Certainly, these rules of thumb work properly with most of the systems. However, in case of a rigid mechanical system (e.g., an industrial robot touching a turbine blade) with a small effective damping in the force controlled direction, these rules do not provide always conservative estimates for stability. Also, they cannot reveal the complex structure of the stability domains in the parameter space.

Recent books published on force control of robot manipulators [9–11] present investigations mainly for the case of continuous-time (analog) force control. A simple model is considered in [9] to investigate some effects caused by the digital force feedback. Experiments validating the proposed control algorithms have usually been carried out using digitally controlled experimental testbeds without further discussing the dynamics of the digitally controlled system [12].

Several researchers had to model deadtime and also the potentially destabilizing sampling effects in order to explain certain stability and low frequency vibration phenomena in digital force control [9,13–15]. These robotic applications were followed by the experiences of the haptics community [16–18]. Recently, intensive research on haptic devices has called the attention to the differences in the dynamic behavior of digital and analog force control systems [19].

Turbine blade polishing is a typical example for the case where digital effects and the variable effective stiffness along the blade caused unexpected vibrations in the system under digital force control [20]. As other reports [21–23] show, more thorough stability analyses are needed when oscillatory systems are to be controlled, which is often the case in force control.

Nowadays, a lot of robotic applications utilize the enormous evolution of digital technology. In comparison with the early 1980s, the speed of the processors and the communication rate between the sensors and the computer seem to be very fast. The sampling rate of the two degrees-of-freedom (DoF) hybrid position/force controller in [3] was set only at 60–120 Hz, while a recently developed force controlled six DoF manipulator with an open controller [11] is sampled at 1 kHz. From the engineering point of view, this kind of sampling

* Corresponding author. Tel.: +36 1 463 3678; fax: +36 1 463 3471.
E-mail addresses: kovacs@mm.bme.hu (L.L. Kovács), jozsef.kovecses@mcgill.ca (J. Kövecses), stepan@mm.bme.hu (G. Stépán).

0020-7462/$ - see front matter © 2008 Elsevier Ltd. All rights reserved.
doi:10.1016/j.ijnonlinmec.2008.04.002

looks almost continuous. Indeed, a digital force control algorithm with a high sampling frequency can be considered "continuous" if the end effector of the robot comes to contact with a relatively soft environment where the effective stiffness of the system is low and the effective mass is high. However, examples for the opposite situation are reported in [16,18,20,24]. Note also that the sampling frequency of industrial robots has not increased as much as the speed of available processors. This is due to the increased complexity of the applied control algorithms and the higher level of programming. In case of either force control with inner position loop or model-based force control, the sampling frequencies are often in the range of 10–50 Hz, only [9,22,25].

When feedback is used in practice, the first attempt is almost always the application of PID controllers. Of course, depending on the given control task, it has non-linear alternatives with superior performance characteristics, but it can be viewed as a simple building block that is often integrated into complex control architectures. For example, as an adaptive extension, a model based controller can be used in supervisory mode over a stable PID controller. Still, there are difficulties in applying simple PID controllers. According to [26], "adding derivative action to a PI controller increases the complexity of the design considerably" and also "there is much folklore concerning derivative action" with especial regard to the appropriate tuning of the control gains. The synthesis of sensors, digital controllers and mechanical devices, i.e., the mechatronic approach to extend the applicability and performance of robotic manipulators, leads to complex system dynamics even in case of simple mechanical structures.

The goal of this paper is to present a detailed stability analysis of a proportional–derivative (PD) digital force control loop considering that the force derivative signal is ideally filtered for high frequency noise. The closed form analysis offers insight into the dynamics of digital force control. This work presents analytical investigations and results in understanding the relations and interactions between the dynamic behavior of the system, the control algorithm and the mechanical parameters. The effects of the control gains and mechanical parameters are presented by means of stability charts. These charts can effectively support the engineering work by showing the range of system parameters for which stable and reliable digital force control could be realized and can help to understand better the possible unexpected behavior of digitally controlled multi-DoF systems.

2. Basic model of force controlled system

2.1. Continuous-time model

The mechanical model shown in Fig. 1 has 1 DoF approximating the behavior of a robotic arm with force control in one direction. The equivalent mass m and the stiffness k can either be identified experimentally or calculated using the constraint Jacobian representing the force controlled direction, and the mass and stiffness matrices of the robot [27]. The generalized force Q represents the effects of the joint drives, while C denotes the magnitude of the effective Coulomb friction force. Similar models are frequently used to analyze force control [6,9]. Differential feedback is widely applied in position control. One of the main objectives of our investigation is to provide a detailed analysis on the effects of the differential gain in the force control loop (see Fig. 1).

In the model of Fig. 1, q_d refers to the position that corresponds to the desired constant force $F_\mathrm{d} = kq_\mathrm{d}$, while $x = q - q_\mathrm{d}$ measures the deformation of the spring relative to this desired position. The equation of motion of the above mechanical model can be written as

$$m\ddot{q}(t) = -kq(t) - C\operatorname{sgn}\dot{q}(t) + Q(t),$$

$$Q(t) = F_m(t) - P(F_m(t) - F_\mathrm{d}) - D\dot{F}_m(t), \tag{1}$$

where P and D are the proportional and the differential gains, respectively. The contact force $F_m(t) = kq(t)$ is measured through the deformation $q(t)$ of the spring. In stiff systems, this signal can be noisy, therefore its derivative $\dot{F}_m(t) = k\dot{q}(t)$ is assumed to be filtered that may cause some delay. If there is no dry friction in the model, the only trivial solution of Eq. (1) is $q(t) \equiv q_\mathrm{d}$. If considerable dry friction can be detected (e.g., at the joints), then there are several equilibriums q^* leading to the steady state force error

$$|\Delta F| = \max_{q^*} |k(q_\mathrm{d} - q^*)| = \frac{C}{P}. \tag{2}$$

Clearly, the higher the proportional gain is, the less the force error is [6]. The accuracy of the control is determined by the maximum proportional gain of the applied PD controller within the limits of stability (for short it is called the maximal stable proportional gain hereafter).

Since dry friction decreases the total mechanical energy during motion, the stability properties of a stable frictionless system do not change in the presence of friction. Thus, the stability analysis in (1) will be carried out with $C = 0$. Introducing the perturbation x around the desired position as $q(t) = q_\mathrm{d} + x(t)$, the equation of motion (1) assumes the form

$$\ddot{x}(t) + D\omega_\mathrm{n}^2\dot{x}(t) + P\omega_\mathrm{n}^2 x(t) = 0, \tag{3}$$

where $\omega_\mathrm{n} = \sqrt{k/m}$ is the natural angular frequency of the uncontrolled mechanical system. According to the Routh–Hurwitz criterion, the solution $x(t) \equiv 0$, and the corresponding contact force $F(t) \equiv F_\mathrm{d}$, is asymptotically stable for any control gains $P > 0, D > 0$. Although the power constraint at the input provides a limit for the control forces, the steady state force error could still be eliminated in principle with large proportional gains.

It is easy to see that the force error expression (2) is preserved also in case of digital control, but the force error cannot be simply eliminated by increasing the proportional gain without the risk of losing stability. This will be explained by analyzing the discrete-time dynamics of the system.

2.2. Discrete-time model

The discrete-time nature of computer controlled systems is considered with a zero-order-hold (ZOH). The digital processor sets the

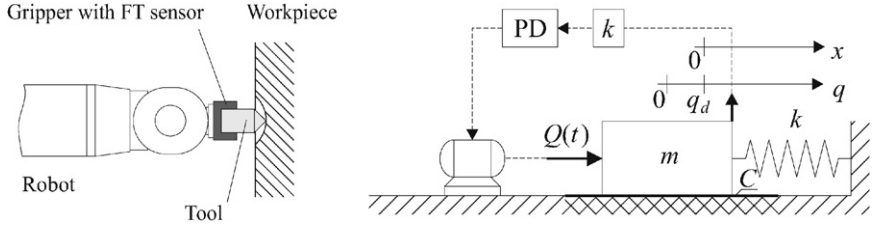

Fig. 1. Mechanical model of unidirectional PD force control.

control output at the time instants $t_n = n\Delta t$, $n = 0, 1, 2, \ldots$, where Δt is the sampling time. In practice, the time derivative of the measured force can be estimated by finite differences sampled at a much higher sampling rate than that of the closed digital control loop. To avoid noisy $\dot{F}_m(t)$ signals, a cascade of low-pass filters can be used [28]. For this reason, we use $\dot{F}_m(t) = k\dot{q}(t) = k\dot{x}(t)$ in our mathematical model as a derivative term. Thus, the control force defined in (1) becomes piecewise constant, and the equation of motion (3) of the controlled system can be rewritten as follows:

$$Q(t) = (1-P)kx((n-1)\Delta t) - Dk\dot{x}((n-1)\Delta t) + kq_{\mathrm{d}}, \tag{4}$$

$$\ddot{x}(t) + \omega_{\mathrm{n}}^2 x(t) = (1-P)\omega_{\mathrm{n}}^2 x((n-1)\Delta t) - D\omega_{\mathrm{n}}^2 \dot{x}((n-1)\Delta t), \quad t \in [n\Delta t, (n+1)\Delta t). \tag{5}$$

Let us introduce the dimensionless time as $T = \omega_{\mathrm{n}} t$, and the notation $T_n = n\Delta T$ for the nth dimensionless sampling instant, where $\Delta T = \omega_{\mathrm{n}}\Delta t$ is the dimensionless sampling time. The equation of motion (5) simplifies to

$$x''(T) + x(T) = (1-P)x_{n-1} - D\omega_{\mathrm{n}} x'_{n-1}, \quad T \in [T_n, T_{n+1}) \tag{6}$$

with prime standing for the dimensionless time derivative. Using the state vector $\mathbf{x} = \mathrm{col}(x\ x')$ and $\mathbf{x}_{n-1} = \mathbf{x}(T_{n-1})$ we can arrange (6) into the matrix form

$$\mathbf{x}'(T) = \mathbf{A}\mathbf{x}(T) + \mathbf{B}\mathbf{x}_{n-1}, \quad T \in [T_n, T_{n+1}), \quad n = 0, 1, 2, \ldots, \tag{7}$$

where the corresponding coefficient matrices have the form

$$\mathbf{A} = \begin{bmatrix} 0 & 1 \\ -1 & 0 \end{bmatrix}, \quad \mathbf{B} = \begin{bmatrix} 0 & 0 \\ 1-P & -D\omega_{\mathrm{n}} \end{bmatrix}. \tag{8}$$

The stability of this state space model is analyzed in closed form in the subsequent section.

3. Stability analysis

3.1. Discrete map

First, we construct a discrete mapping possessing the same stability properties as that of (7) [4]. The general solution of the non-homogeneous system (7) is

$$\mathbf{x}(T) = \mathrm{e}^{\mathbf{A}(T-T_n)}\mathbf{c} - \mathbf{A}^{-1}\mathbf{B}\mathbf{x}_{n-1}, \quad T \in (T_n, T_{n+1}], \tag{9}$$

where the substitution of the initial conditions $\mathbf{x}(T_n) = \mathbf{x}_n$ yields the coefficient vector

$$\mathbf{c} = \mathbf{x}_n + \mathbf{A}^{-1}\mathbf{B}\mathbf{x}_{n-1}. \tag{10}$$

Thus, the state variables at the end of the nth sampling interval can be calculated as

$$\mathbf{x}_{n+1} = \mathrm{e}^{\mathbf{A}\Delta T}\mathbf{x}_n + (\mathrm{e}^{\mathbf{A}\Delta T} - \mathbf{I})\mathbf{A}^{-1}\mathbf{B}\mathbf{x}_{n-1}. \tag{11}$$

Its scalar form

$$\begin{aligned} x_{n+1} &= x_n \cos\Delta T + x'_n \sin\Delta T + (1-\cos\Delta T) \\ &\quad \times ((1-P)x_{n-1} - D\omega_{\mathrm{n}} x'_{n-1}), \\ x'_{n+1} &= -x_n \sin\Delta T + x'_n \cos\Delta T \\ &\quad + \sin\Delta T((1-P)x_{n-1} - D\omega_{\mathrm{n}} x'_{n-1}) \end{aligned} \tag{12}$$

leads naturally to the following choice of a three-dimensional discrete state vector:

$$\mathbf{x}_n = \mathrm{col}((1-P)x_{n-1} - D\omega_{\mathrm{n}} x'_{n-1}\ \ x_n\ \ x'_n). \tag{13}$$

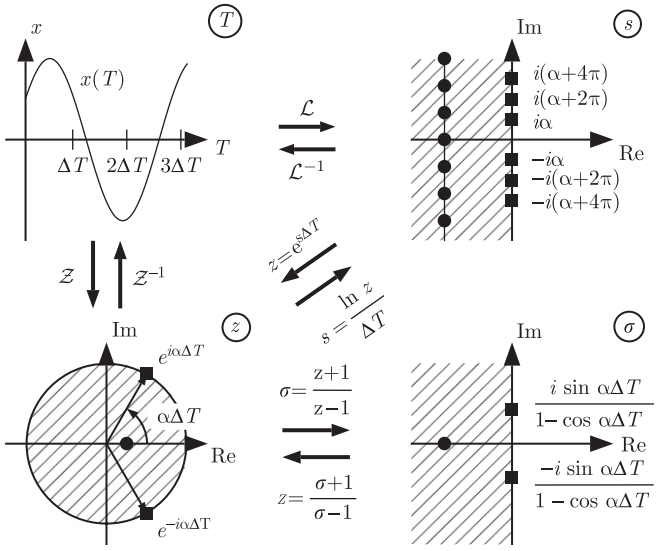

Fig. 2. Transformations used in this paper.

Based on this, Eq. (11) can be rewritten as

$$\mathbf{x}_{n+1} = \mathbf{H}\mathbf{x}_n, \quad \mathbf{H} = \begin{pmatrix} 0 & 1-P & -D\omega_{\mathrm{n}} \\ 1-\cos\Delta T & \cos\Delta T & \sin\Delta T \\ \sin\Delta T & -\sin\Delta T & \cos\Delta T \end{pmatrix} \tag{14}$$

which represents a generalized three-dimensional geometric series. The convergence of (14) is equivalent to the asymptotic stability of the force control described by (7). The stability of the system is determined by the eigenvalues z of the transition matrix $\mathbf{H}$. However, the study of the possible bifurcations and vibration frequencies along the stability limits also require the use of the characteristic exponents s. Their relations are represented in Fig. 2 in accordance with the following standard calculation.

The substitution of the exponential trial solution $\mathbf{x}(T) = \mathbf{K}\mathrm{e}^{sT}$ ($s \in \mathbb{C}, \mathbf{K} \in \mathbb{R}^3$) into (14) yields the characteristic equation $\det(\mathrm{e}^{s\Delta T}\mathbf{I} - \mathbf{H}) = 0$. This has an infinite number of roots s_k, $k = 1, 2, \ldots$ called characteristic exponents, which are situated along a finite number of vertical lines in the complex plane as shown in Fig. 2 [4]. Clearly, there is only a finite number of characteristic multipliers defined by $z = \mathrm{e}^{s\Delta T}$. These are, actually, the three eigenvalues of the transition matrix $\mathbf{H}$. The criterion for the exponential stability of the force control can be written as

$$\det(z\mathbf{I} - \mathbf{H}) = 0, \quad |z_{1,2,3}| < 1 \ \Leftrightarrow\ \mathrm{Re}\, s_k < 0, \quad k = 1, 2, \ldots . \tag{15}$$

The same stability condition is derived in books like [4,7,29] using the Laplace transformation $\mathscr{L}$ and the $\mathscr{Z}$-transformation, which are also illustrated in Fig. 2, but the form of $\mathbf{H}$ is given in (14) only.

3.2. Stability charts

As shown in Fig. 2, the bilinear transformation $z = (\sigma+1)/(\sigma-1)$ [4,29] maps the open unit disk back into the left half of the complex plane. Thus, the stability condition (15) is formulated for the polynomial

$$p_3(\sigma) = (\sigma-1)^3 \det\left(\frac{\sigma+1}{\sigma-1}\mathbf{I} - \mathbf{H}\right) = \sum_{i=0}^{3} b_i \sigma^i, \tag{16}$$

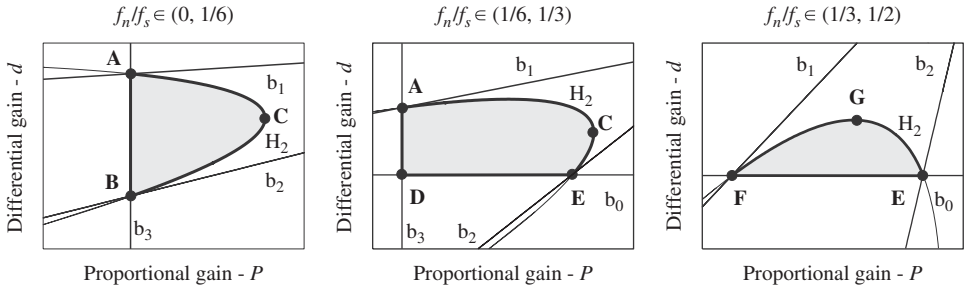

Fig. 3. Possible shapes of the P–d stability charts.

where the Routh–Hurwitz criterion can be applied directly for the coefficients

$$b_3 = P(1-\cos\Delta T),$$
$$b_2 = D\omega_n \sin\Delta T + (3-2P)(1-\cos\Delta T),$$
$$b_1 = -2D\omega_n \sin\Delta T + (2-P)\cos\Delta T + P,$$
$$b_0 = D\omega_n \sin\Delta T + \cos\Delta T + 1. \tag{17}$$

The stability charts are constructed in the space of three, dimensionless variables

$$P, d = \omega_n D \quad \text{and} \quad \frac{f_n}{f_s} = \frac{\omega_n/2\pi}{1/\Delta t} = \frac{\Delta T}{2\pi}, \tag{18}$$

where P and d are the dimensionless proportional and differential gains, respectively, while f_n/f_s is the ratio of the natural frequency of the uncontrolled mechanical system and the sampling frequency of the control.

For the coefficients in (17) and $H_2 = b_1 b_2 - b_3 b_0$, the Routh–Hurwitz criterion yields the following necessary and sufficient exponential stability conditions:

$$b_3 > 0 \;\Leftrightarrow\; P > 0 \quad \text{and} \quad f_n/f_s \neq k, \;\; k = 0, 1, 2\ldots, \tag{19}$$

$$b_2 > 0 \;\Leftrightarrow\; d > \frac{(2P-3)(1-\cos\Delta T)}{\sin\Delta T}, \tag{20}$$

$$b_1 > 0 \;\Leftrightarrow\; d < \frac{(2-P)\cos\Delta T + P}{2\sin\Delta T}, \tag{21}$$

$$b_0 > 0 \;\Leftrightarrow\; d > -\frac{\cos\Delta T + 1}{\sin\Delta T} \quad \text{and} \quad f_n/f_s \neq 2k+1, \quad k = 0, 1, 2\ldots, \tag{22}$$

$$\begin{aligned} H_2 > 0 \;\Leftrightarrow\; 0 < {} & -2(1-\cos\Delta T)^2 P^2 \\ & + 2(1-\cos\Delta T)(2d\sin\Delta T - 4\cos\Delta T + 1)P \\ & + 2(\cos\Delta T - d\sin\Delta T) \\ & \times (d\sin\Delta T + 3(1-\cos\Delta T)). \end{aligned} \tag{23}$$

Based on these equations, we can perform the detailed stability analyses of the model. In the plane of the control parameters P and d, the resulting stable domain is bounded by the straight lines $b_1 = 0$ and $b_3 = 0$ together with the implicitly defined parabola $H_2 = 0$. Depending on the value of the frequency ratio chosen in $(0, \frac{1}{2})$, three possible shapes can be determined for the stable domains shown shaded in Fig. 3. The coordinates of the characteristic points A…G of the charts are given in closed form in Table 1. Among these points, we can find the maximum proportional gain at C or E. These formulas and stability charts have importance at the design stage of force control to synchronize basic mechanical and control parameters.

Table 1
Characteristic points of the P–d stability charts

	Proportional gain	Differential gain
A	0	$\frac{1}{\tan\Delta T}$
B	0	$-\frac{3(1-\cos\Delta T)}{\sin\Delta T}$
C	$\frac{(2\cos\Delta T-3)^2}{8(1-\cos\Delta T)}$	$\frac{(2\cos\Delta T+3)(2\cos\Delta T-1)}{8\sin\Delta T}$
D	0	$-\frac{1+\cos\Delta T}{\sin\Delta T}$
E	$\frac{1-2\cos\Delta T}{1-\cos\Delta T}$	$-\frac{1+\cos\Delta T}{\sin\Delta T}$
F	$-\frac{2+4\cos\Delta T}{1-\cos\Delta T}$	$-\frac{1+\cos\Delta T}{\sin\Delta T}$
G	$\frac{(2\cos\Delta T-1)(2\cos\Delta T-5)}{8(1-\cos\Delta T)}$	$\frac{(2\cos\Delta T+1)^2}{8\sin\Delta T}$

In order to see the structure of the stable domains for frequency ratios in the range of $(\frac{1}{2}, 1)$ and further, we also construct $f_n/f_s - P$ charts shown in Fig. 4 for three different values of dimensionless differential gains. These charts are periodic in the frequency ratio with periodicity 1 (see later at Fig. 5).

We note that this periodicity may not have great significance for several practical applications. This is because, according to Shannon's sampling theorem [7], frequency ratios greater than $\frac{1}{2}$ should be avoided. However, regardless of this, the periodicity of the stability charts can still be seen as an important physical phenomenon observed in mechanical systems with digital force feedback. For example, it can have practical importance in applications where the sampling frequency is limited by the hardware.

The first chart in Fig. 4 shows a simple proportional controller, i.e., d=0, where the maximal stable proportional gain is 1.5. According to (2), this means that the steady state force error cannot be guaranteed to be below 66% of the magnitude of the generalized friction force in the system.

In contrast, when d has a relatively high positive value, the upper limit of the stable domain tends to infinity in a narrow range of low frequency ratios. In principle, this gives the possibility to eliminate the steady state error of a digital force controller. In practice, this can be difficult to achieve because, apart of the power constraint at the input, the stable domain becomes narrow with respect to the frequency ratio. This narrow stable domain also shows up at $f_n/f_s = 1+, 2+, \cdots$ (see Fig. 5).

Another important property of the charts presented in Fig. 4 is that the stable domains become disjoint and some of them disappear by increasing the differential gain. For high differential gains, only narrow stable domains exist at certain frequency ratios. This can offer an explanation for why the differential gain is avoided in practice even when the noisy force derivative signal is properly filtered.

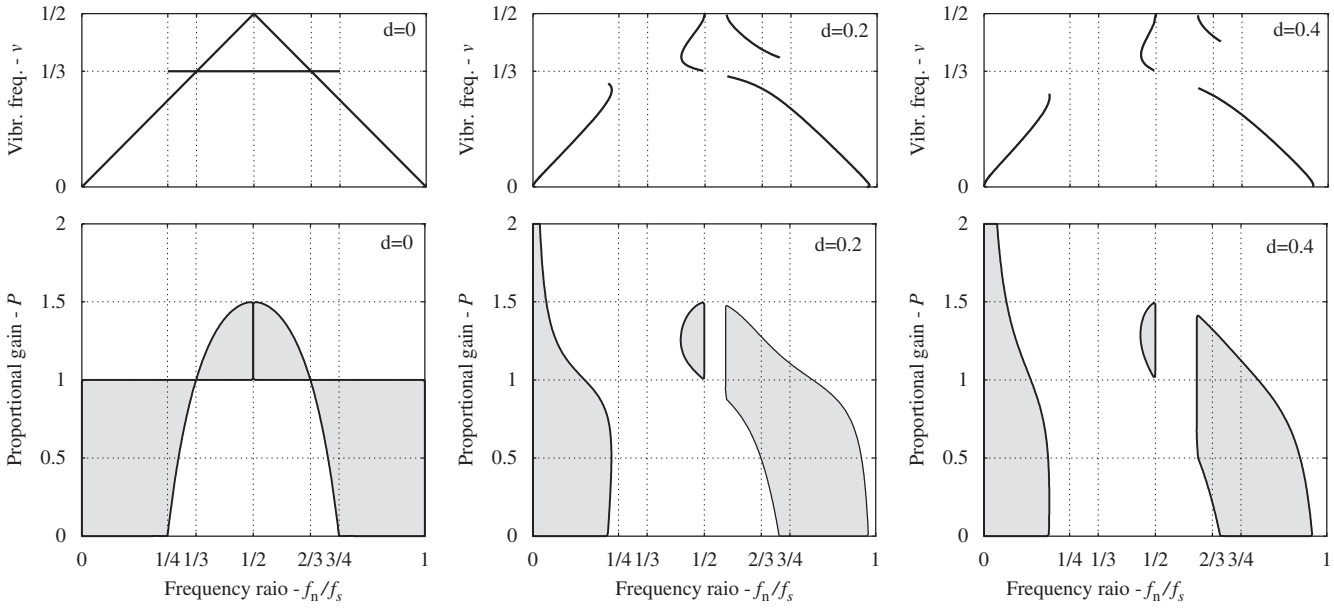

Fig. 4. The $f_n/f_s - P$ stability charts.

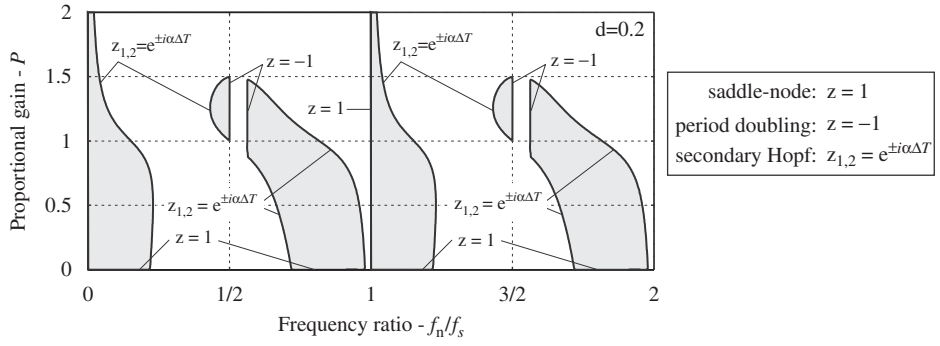

Fig. 5. The three different kinds of possible bifurcations.

4. Dynamic behavior

In the case of discrete-time systems, three different kinds of bifurcation may occur along the stability limits [30]. The characteristic multiplier z may cross the unit circle at -1, at $+1$, or at a complex conjugate pair $z_{1,2}=\exp(\pm i\alpha\Delta T)$. As an illustration, the $f_n/f_s - P$ chart corresponding to $d=0.2$ is presented in Fig. 5 showing the periodic nature of the stable regions and also the three kinds of bifurcations mentioned above.

If we substitute $z=1$ into the characteristic polynomial in (15), the resulting expression is $b_3=0$. Using Eq. (17), $b_3=0$ is satisfied when $f_n/f_s = k,\ k=1,2,\ldots$, or $P=0$. Along these stability limits, saddle-node bifurcation may occur [30]. In the case of $P=0$, the physical meaning of this bifurcation is obvious: the control works in the opposite way, of course, for negative gains.

The substitution of $z=-1$ into the characteristic polynomial in (15) yields $b_0=0$. This equation can be solved using (17). These boundaries refer to period-doubling bifurcations [30]. In this case, the system starts to oscillate with the period of $2\Delta t$, which is just the double of the sampling time. Among the corresponding stability boundaries, we can find the straight lines characterized by $f_n/f_s = 0.5 + k,\ k=1,2,\ldots$, which are independent of the value of the differential gain.

In the third case, when $z_{1,2}=\exp(\pm i\alpha\Delta T)$, the secondary Hopf (or Neimark–Sacker) bifurcation [30] may occur along the stability limit $H_2=0$ (see formula (23)). This kind of bifurcation is the most typical in practical cases (see Fig. 5), when self-excited vibrations are experienced. Fig. 2 shows that the frequencies of these vibrations can be obtained by the inverse of the definition of characteristic multipliers $s=\ln z/\Delta T$. This transformation maps the unit circle of the complex plane into the imaginary axis, where $\alpha \pm k\pi,\ k=1,2,\ldots$ give the different vibration frequencies of the developing oscillatory motion in the dimensionless time domain. It is easy to see that there are infinitely many of these vibration frequency components. Physically, the lowest one is the most important, since it has the strongest peak in the spectrum.

The relative vibration frequencies $v=(\alpha\omega_n/(2\pi))/(1/\Delta t)=\alpha f_n/f_s$ corresponding to these relevant lowest frequencies α are shown above the stability charts in Fig. 4. The highest values of v are at $f_s/2$ (the half of the sampling frequency), where the stability bounds associated with the secondary Hopf bifurcations intersect the stability bounds related to the period doubling bifurcations.

An important consequence of these results is that the system will oscillate at a relatively low frequency when it loses its stability along the limit $H_2=0$. This could be the case in practice when the proportional gain is increased to achieve a better accuracy at low

frequency ratios. As was already mentioned in the introduction, these unexpected low frequency vibrations are reported in several papers [14,15,31]. For small frequency ratios, the frequency of the possible vibrations is far smaller than the sampling frequency of the controller no matter if a differential gain is applied or not. In the case, when a PD controller is applied and the sampling frequency and the proportional gain are both set to be high in order to improve the accuracy of the control, the frequency of the possible vibrations is only 10–15% of the sampling frequency.

5. Conclusions

The dynamics of mechanical systems with digital force control was investigated in this paper. Many undesired events in force controlled systems (e.g., instability, oscillations) are often explained by referring to "unmodelled high frequency dynamics", but some of these events are caused directly by the discrete-time nature of the controller. The underlying physical cause for the stability problems having unexpected parameter dependences in force control is the peculiar behavior of the so-called delayed oscillator [32]. It is well known that the discrete-time controller introduces time delay, which can have destabilizing effects depending on the system parameters. In case of second order systems, like an oscillator with low viscous damping, the parameter dependence is intricate. Since robotic force control is often applied to systems of large stiffness and low damping, vibration problems are typical in practice.

In this paper, particular attention has been paid to the effects of the differential gain. The differential gain is commonly used in position control, but it has usually been avoided in force control without much analytical explanation. In this work, detailed stability and performance analyses were carried out to characterize the derivative feedback term under the condition that the force derivative signal is ideally filtered. The main effects of the differential gain are summarized in the following:

- As illustrated in Fig. 4, introducing a differential gain will reduce significantly the area of the stable domains in the $f_n/f_s - P$ (natural frequency and sampling frequency ratio – proportional gain) stability charts.
- By adding a differential gain, the stability domains become disjoint and narrow (see Fig. 4). There are certain frequency ratios where no stable control is possible with a fixed differential gain in the control. The narrow stable domains become very elongated along the P-axis. The proportional gain can be further increased within the limits of stability to minimize the steady state force error, but the system becomes very sensitive even to slight frequency parameter variations.
- The dynamic behavior of the system in the neighborhood of the stability boundaries can lead to three different kinds of bifurcations. The two relevant ones are the period-doubling and the secondary Hopf bifurcations. Typically, these lead to self-excited low frequency oscillations with frequencies of 10–15% of the sampling frequency, but they will always be less than the 50% of the sampling frequency. The differential gain does not have a dominant influence on these low vibration frequencies, but it makes the self-excited vibration frequencies even less likely to be in the 30–50% region of the sampling frequency (see Fig. 4).

The stability charts are periodic as the frequency ratio is increased, the stable domains are repeated in every $(k, k+1),\ k \in \mathbb{N}^+$ intervals of the frequency ratio. At properly tuned low sampling frequencies, it is still possible to select gains under which the system becomes stable, while the periodic nature also implies that at high sampling frequencies, the system can loose its stability if the gains are not selected properly. The proper tuning and selection of the control gains are equally important for both low and high sampling frequencies, especially when the force controlled mechanical system has many natural frequencies with low modal damping ratios. The periodicity of the stability charts is an interesting physical phenomenon in mechanical systems with digital force feedback. However, we have to note that for practical systems the frequency ratio should be kept below $\frac{1}{2}$ according to Shannon's sampling theorem.

Most of the investigations were based on the assumption of the availability of the time derivative of the measured force. In practice, however, this derivative can be approximated using finite differences of measured force values, which also provide some kind of filtering. The more detailed analysis of this finite difference approximation shows that the above conclusions still hold if the force sensor's internal sampling frequency is high enough.

Acknowledgments

This research was done within the frame of the Bilateral Hungarian–Canadian Society and Technology Program under Grant no. TéT-BILAT CAN-1/03. It was also supported by the Hungarian Scientific Research Foundation under Grant no. K68910, and by the Natural Sciences and Engineering Research Council of Canada under Grant no. 298206-04.

References

[1] D.E. Whitney, Force feedback control of manipulator fine motions, ASME J. Dyn. Syst. Meas. Control 98 (1977) 91–97.
[2] D.E. Whitney, Historical perspective and state of the art in robot force control, Int. J. Robot. Res. 6 (1) (1987) 3–14.
[3] M.H. Raibert, J.J. Craig, Hybrid position/force control of manipulators, ASME J. Dyn. Syst. Meas. Control 102 (1981) 126–133.
[4] B.C. Kuo, Digital Control Systems, SRL Publishing Company, Champaign, IL, 1977.
[5] R. Isermann, Digital Control Systems, Springer, Berlin, 1981.
[6] J.J. Craig, Introduction to Robotics Mechanics and Control, Addison-Wesley, Reading, MA, 1986.
[7] K.J. åström, B. Wittenmark, Computer-Controlled Systems: Theory and Design, second ed., Prentice-Hall, Upper Saddle River, NJ, 1990.
[8] J.J.E. Slotine, W. Li, Applied Nonlinear Control, Prentice-Hall Inc., Englewood Cliffs, NJ, 1991.
[9] D.M. Gorinevsky, A.M. Formalsky, A.Y. Schneider, Force Control of Robotics Systems, CRC Press LLC, Boca Raton, FL, 1997.
[10] B. Siciliano, L. Villani, Robot Force Control, Kluwer Academic Publishers, Dordrecht, 1999.
[11] C. Natale, Interaction Control of Robot Manipulators, Springer, Berlin, Heidelberg, 2003.
[12] S. Chiaverini, B. Siciliano, L. Villani, A survey of robot interaction control schemes with experimental comparison, IEEE/ASME Trans. Mechatronics 4 (3) (1999) 273–285.
[13] J. Baeten, J.D. Schutter, Integrated Visual Servoing and Force Control, Springer, Berlin, Heidelberg, 2003.
[14] G. Stépán, A. Steven, L. Maunder, Design principles of digitally controlled robots, Mech. Mach. Theory 25 (1990) 515–527.
[15] A. Steven, J.R. Hewit, Hybrid position and force control applied to robotic polishing of turbine blading, in: Proceedings of the Third International Conference on Advanced Robotics (ICAR 1987), Versailles, 1987, pp. 493–502.
[16] J.E. Colgate, G.G. Schenkel, Passivity of a class of sampled-data systems: application to haptic interfaces, J. Robot. Syst. 14 (1) (1997) 37–47.
[17] G.R. Luecke, Y.H. Chai, Stability and performance comparison of the force reflecting haptic manipulator, in: Proceedings of the Eighth International Conference on Advanced Robotics (ICAR'97), Monterey, CA, 1997, pp. 637–642.
[18] R.J. Adams, M.R. Moreyra, B. Hannaford, Stability and performance of haptic displays: theory and experiments, in: Proceedings of the ASME International Mechanical Engineering Congress and Exhibition, Anaheim, CA, 1998, pp. 227–234.
[19] J.J. Gil, A. Avello, Á. Rubio, et al., Stability analysis of a 1 DOF haptic interface using the Routh–Hurwitz criterion, IEEE Trans. Control Syst. Technol. 12 (4) (2004) 583–588.
[20] G. Stépán, A. Steven, L. Maunder, Dynamics of robots with digital force control, in: Proceedings of CSME Mechanical Engineering Forum 1990, vol. 3, Toronto, 1990, pp. 355–360.
[21] L. Whitcomb, S. Arimoto, T. Naniwa, et al., Experiments in adaptive model-based force control, IEEE Control Syst. 16 (1) (1996) 49–57.
[22] L.L. Kovács, G. Stépán, Dynamics of digital force control applied in rehabilitation robotics, Meccanica 38 (2) (2003) 213–226.

[23] H. Xu, A. Datta, S.P. Bhattacharyya, Computation of all stabilizing PID gains for digital control systems, IEEE Trans. Automat. Control 46 (4) (2001) 647–652.
[24] G. Stépán, G. Haller, Quasiperiodic oscillations in robot dynamics, Nonlinear Dyn. 8 (1995) 513–528.
[25] R.G. Landers, A.G. Ulsoy, Model-based machining force control, J. Dyn. Syst. Meas. Control 122 (3) (2000) 521–527.
[26] K.J. åström, T. Hägglund, The future of PID control, Control Eng. Practice 9 (11) (2001) 1163–1175.
[27] J. Kövecses, J.C. Piedboeuf, C. Lange, Dynamics modeling and simulation of constrained robotic systems, IEEE/ASME Trans. Mechatronics 8 (2) (2003) 165–177.
[28] JR3, Inc. DSP based receiver architectural overview. URL: ⟨http://www.jr3.com/arch.html⟩, access date: 12/04/2007.
[29] K. Ogata, Discrete-Time Control Systems, Prentice-Hall, Englewood Cliffs, NJ, 1995.
[30] J. Guckenheimer, P. Holmes, Nonlinear Oscillations, Dynamical Systems, and Bifurcation of Vector Fields, Springer, New York, 1986.
[31] Y. Chen, Frequency response of discrete-time robot systems, in: Proceedings of IEEE Conference on Robotics and Automation, Raleigh, 1987, pp. 464–472.
[32] S.I. Niculescu, Delay Effects on Stability: A Robust Control Approach, Springer, Berlin, 2001.